DOI: https://doi.org/10.24297/jap.v15i0.8015

Dielectric and Electrical Properties of Poly (E-Caprolactone)/ Organomodified Clay Bionanocomposites Prepared in Open Air by in Situ Polymerization

S. Hrichi[1*], M. Arous[1], M. Raihane[2], M. Lahcini[2], H. Elghoui[2], F Z. Bouharras[2], A. Kallel[2]

[1] LaMaCoP, Faculty of Sciences of Sfax, University of Sfax, BP 802-3018 Sfax, Tunisia

[2] Laboratory of Organometallic and Macromolecular Chemistry-Composites Materials, Faculty of Sciences and Technologies, Cadi-Ayyad University, 40000 Marrakech, Morocco

soulefhrichi@yahoo.fr

ABSTRACT

Dielectric and electrical properties of bio-nanocomposites based on poly (ε-caprolactone) (PCL) with different amounts of organomodified montmorillonite clay (MMT-ODA) were investigated by broadband dielectric spectroscopy in the frequency range from 1Hz to 1MHz and in the temperature range from -100 to 25°C. These nanocomposites were prepared by in situ Ring Opening polymerization of ε-caprolactone in open air by using titanium alkoxide as a catalyst. Due to the semicrystalline structure of PCL, the high number of modes and its overlap, the relaxation patterns observed on dielectric spectra were complicated. These relaxation data were modeled using the H-N empirical equation with the contribution of conductivity. The local dynamics of PCL were unaffected by the increase of nano-clay amount, in agreement with the DSC values of glass transition temperature. The PCL/MMT-ODA 3 wt% exhibited the lowest value of dielectric strength, indicating the strongest adhesion between PCL matrix and organo-modified clay. As for PCL/MMT-ODA 5 wt%, the presence of agglomerate made the adhesion between PCL and MMT-ODA very weak. The obtained findings were congruent FTIR and XRD results. The electrical conductivity of PCL was analysed according to the Jonscher's law. The obtained exponent s values referred to three models corresponding to different temperature ranges.

Keywords: bionanocomposites; polycaprolactone; montmorillonite; organomodified clay; dielectric properties; electrical conductivity.

1. Introduction

Synthetic polymers are artificial macromolecular substances that have witnessed colossal progress in terms of variety and quantity during the last decades. Owing to the scientific and technological progress, they have been widely used in almost all areas of human activity. Generally, this type of polymers is non-degradable and the vast majority is made from non-renewable fossil fuels. Face to the depletion of petroleum resources and the adverse environmental problems caused by the temporary use of these polymers, many governments are launching initiatives to encourage the research on biodegradable polymers and its development. And since the 1970s, biodegradable polymeric materials, which could be cleaved by microorganisms such as bacteria in carbon dioxide and water biological or chemical reactions [1-4], have received a lot of attention. Therefore, to extend their applications, they have been associated with nano-fillers, which could bring a large range of improved properties (stiffness, permeability, crystallinity, thermal stability, etc.), compared to pure polymers or macro- and micro-composites [5-8]. The nanocomposites based on biodegradable polymers and nano-charges, known as bio-nanocomposites, have been the topic of many researches. Layered silicates as nano-charges and biopolymers as matrix, are currently the most promising bio-nanocomposites for a wide range of important applications [5]. In particular, the aliphatic polyesters have been the subject of increasing focus because of their biodegradability, biocompatibility and non-toxicity. Poly (ε-caprolactone) (PCL) is one of the best candidates. It is semi-crystalline linear and biodegradable polyester [9] with a low glass transition temperature (T_g = -60°C). Much research effort has been devoted to the thermal, mechanical, structural,

morphological and dielectric properties of PCL and/or nanocomposites based on PCL and natural nano-charge. However, works on its electrical properties, reported so far, are limited. Grimau et al [10] and Bello et al [11] studied the dielectric properties of PCL using permittivity ε* and modulus M* formalism, respectively. Bello [11] highlighted low frequency- high temperature interfacial polarization in addition to the segmental mode α relaxation and local modes β and γ previously addressed by Grimau et al [10]. Woo et al [12] concentrated on the thermal and conduction properties of proton conducting polymer electrolyte based on PCL. Kevin et al [13] analyzed the dielectric spectra of PCL blended with small amounts of Cloisite 30B nanoplatelets. They noted a minimal Cloisite impact on vitreous state dynamics and the segmental dynamics, explained by weak interactions between polymer and platelets. Avella et al [14] prepared PCL based nanocomposites by the extrusion process and reported the effect of silica nanoparticles on thermal, morphological and mechanical properties of these samples.

In our study, the ε-caprolactone (ε-CL) has been polymerized in the presence of montmorillonite nanoclay (MMT). The MMT clay modification by octadecylamine (ODA) is necessary to render it more organophilic, increase its interlayer spacing and promote its compatibility with the PCL matrix. Therefore, these organic compounds (polar solvents and polymers) may easily enter the galleries of the interlayers [15]. Interstingly, the polymerization was carried out in open air by using titanium alkoxide as a catalyst.

The aim of this paper is to study the dielectric and electrical properties of PCL matrix. The influence of added clay in the dielectric permittivity and the conduction mechanism were discussed.

2. Materials and Methods

2.1 Materials

The ε-caprolactone was supplied by Alpha Aesar and distilled under reduced pressure from calcium hydride (CaH_2) before use. Hydrochloric acid (HCl) (37%) was provided by Alpha Aesar. Toluene solvent was purified by vacuum distillation over sodium and benzophenone, Titanium tetraisopropoxide ($Ti(OiPr)_4$) was provided by Sigma-Aldrich and used as a catalyst without prior purification. The unmodified montmorillonite (Sigma Aldrich, 99%) noted MMT-Na (cation exchange capacity =92 meq/100g) was dried at 80 °C under vacuum for 24 h. This clay was organomodified by octadecylamine (CH_3 $(CH_2)_{17}$-NH_2) (ODA) in acidic medium to make the organophilic clay and improve the monomer/clay interaction. The modified clay (MMT-ODA) was prepared by the cationic exchange process where the sodium ions Na^+ in the MMT were exchanged with octadecylammonium ions in aqueous solution according to the procedure reported in literature [16].

All samples were prepared by an in situ Ring Opening Polymerization (ROP) reaction using a titanium alkoxide $Ti(OiPr)_4$ due to its stability in open air.

A desired amount of organoclay (0, 2, 3 and 5 wt%) of organomodified clay ODA-MMT was dispersed first in 50 mmol (5.7 ml) of ε-caprolactone (CL) under ultrasound (45% amplitude) for 30 min, and then by magnetic stirring for 24 h at room temperature was dispersed first. The catalyst titanium isopropoxide $Ti(OiPr)_4$ was then added to the mixture, the molar ratio [monomer/initiator] was equal to 5000. The addition of this small quantity requires the preparation of a stock solution of the catalyst in dry toluene. The polymerization was carried into an oil bath preheated at 130 °C and then stirred for 24 h. Finally, the nanocomposite was then removed from the reactor and dried under vacuum at 70 °C for one day.

2.2 Methods

FTIR

FTIR analysis was used to characterize the functional groups of PCL and its nanocomposites. The IR spectra were determined using the Perkin Elmer spectrophotometer within the wave number range from 1000 to 3500 cm^{-1} operating at a resolution of 1 cm^{-1}.

XRD

XRD analysis was used to analyse the organomodification of MMT as well as its dispersion in the nanocomposites. XRD patterns were collected using a Bruker diffractometer (D8 Advance model), equipped with a Cu Kα generator (λ = 1.54 Å). The generator tension and current were 40 kV and 40 mA, respectively. Bragg's equation was used to calculate the basal spacing (d_{001}) for the various MMT-based materials.

DSC

Differential scanning calorimetry (DSC) was used to determine the glass transition temperature (T_g) of PCL and its nanocomposites. We use a Perkin Elmer DSC-7 instrument. DSC measurements were performed on 10-14 mg samples under nitrogen atmosphere. Samples were heated from -80 to -30°C at 10°C min^{-1} (1^{st} heating), cooled to -80°C at the same scan rate, then heated again to -30 at 10°C min^{-1} (2^{nd} heating). From the midpoint value of the jump in heat flow in the second heating run, the Tg value of each sample could be determined. Pyris software was used in the construction of the lines.

TGA

TGA analysis was used to calculate the characteristic temperature of degradation T_d10% (temperature at which 10% degradation occurred), using a Mettler Toledo TGA apparatus (SDTA 851 model). A sample (8 mg) was heated at 10° C min^{-1} under air. TGA curves were recorded from 30 to 900 °C.

Dielectric measurments

Broadband dielectric relaxation spectroscopy was used to investigate the influence of organo-modified clay on the dielectric properties of PCL. The dielectric measurements were performed on samples metalized by gold to improve the contact with the electrodes. First, the sample is placed between two parallel electrodes in the active cell. Measurements were performed under a sinusoidal applied voltage of 1V. The temperature range was from -100 to 25°C with a heating rate of 5°C/min and the measured frequency range was from 10^{-1} Hz until 10^6 Hz. Data acquisition was conducted automatically via suitable software (Windata). This analysis permits to determine the real and the imaginary parts of the generalized complex dielectric permittivity defined by:

$$\varepsilon^*(\omega) = \varepsilon'(\omega) - i\varepsilon''(\omega) \quad (1)$$

where ε′ is interpreted as the polarization term and ε″ designs the global loss factor.

3. Results and discussion

3.1 Structural Characterizations

Fig.1 shows The FTIR spectra of PCL and its bio-nanocomposites. As showing, The bio-nanocomposites followed the same FTIR spectra and the characteristic bands were appearing at the same wave number, as neat PCL, in the 1000-3500 cm^{-1} region at room temperature. The absorption bands at 2945 cm^{-1} and 2867 cm^{-1} were attributed to the characteristic $-CH_2$ asymmetric and symmetric stretching vibration of PCL, respectively. The peak at 1722 cm^{-1} was assigned to the carbonyl -C=O stretching and 1293 cm^{-1} to the C-O and C-C stretching in the crystalline phase. At 1238 cm^{-1} and 1168 cm^{-1}, the presence of the asymmetric and symmetric C-O-C stretching were shown, respectively. These characteristic peaks were observed and confirmed by other studies for PCL samples [12, 17-20]. There was no peak shifting or formation of a new peak to clay supplementation in the nanocomposites, indicating that there were no strong interactions or bonding between PCL and MMT-ODA. These results were in agreement with other observations that concerned PCL based nanocomposite spectra [21, 22].

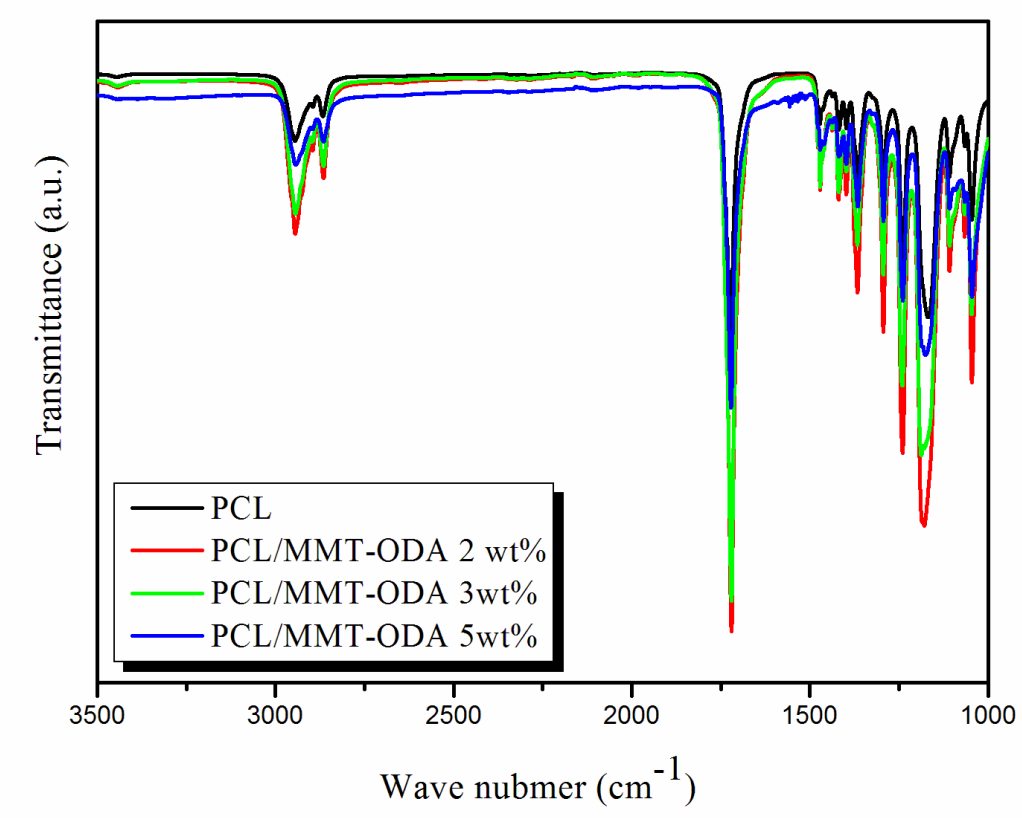

Fig. 1 FTIR spectra recorded at room temperature of neat PCL and its nanocomposites.

It is clear that the intensity of all characteristic bands increased after the addition of modified clay from 0 to 3 wt%. This could be caused by the good dispersion of the clay nanoparticles in the neat matrix. However, for the bio-nanocomposite with 5 wt%, we observed a decrease in the bands intensities. This decrease could be explained by the poor dispersion of MMT-ODA layers within the PCL polymer matrix. At higher loading amount of modified clay, the filler-filler interactions increase and form aggregates, thus the intercalation of PCL chains in the interlayer clay is more difficult. Similar results were reported by Salehiyan et al. [23], they concluded that the reduction of organoclay dispersion was attributed to the filler-filler interactions of modified clay at higher filler loading resulting in agglomerates, and therefore hindering the penetration of polymer into the organoclay gallery.

XRD diffractograms of the clay before (MMT-Na) and after modification clay (MMT-ODA) are displayed in **Fig.2 (a)**. The d-spacing of MMT-Na (d_{001}) diffraction peak was 1.17 nm (2θ= 8°), which was increased to 1.78 nm (2θ= 5°), as modified by ODA.

The XRD diffractograms of PCL/MMT-ODA nanocomposites loading with 2, 3, and 5 wt% are shown n in **Fig.2 (b)**. The d-spacing of MMT-ODA (d_{001}) (1.78 nm) was clearly disappeared in the PCL/MMT-ODA 2 wt% sample. In the case of PCL/ MMT-ODA 3w% and PCL/ MMT-ODA 5 w% samples, broad basal reflections were detected at lower 2-theta angles. The corresponding calculated d-spacing values were read at 3.52 and 3.86 nm respectively, comparatively to 1.78 nm in modified MMT-ODA suggesting intercalated structures in the PCL polymer matrix. In addition, the intensity of the XRD peak was increased with the percentage of MMT-ODA concentration. Due to an increase in clay concentration, the agglomerated clay structures became denser in the polymer matrix and polymer-clay interactions did not overcome the Vander Waals forces between silicate interlayers resulting in incomplete delamination of clay layers.

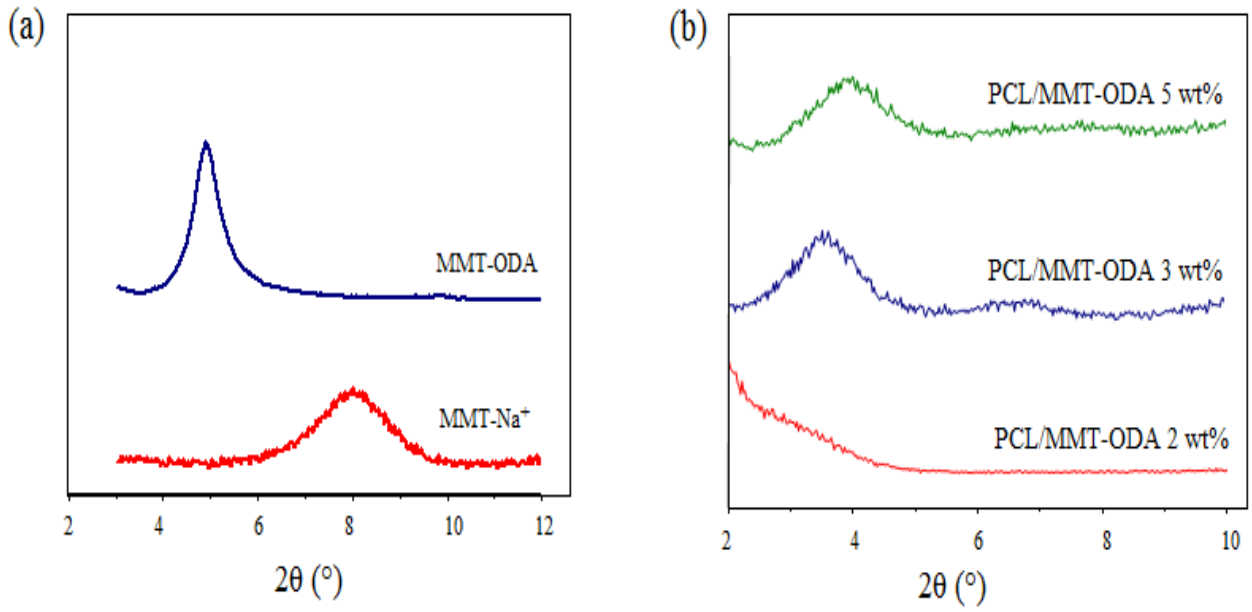

Fig. 2 XRD diffractograms for MMT-Na^+ and MMT-ODA (a) and PCL/ODA-MMT nanocomposites (b).

3.2 Thermal properties

The glass transition temperature (T_g) of PCL and its nanocomposites was determined by Differential scanning calorimetry (DSC) (**Fig.3 (a)**.). The obtained values of the glass to rubber transition temperature at midpoint from the DSC thermographs are summarized in **Table 1**. PCL has a glass transition temperature T_g = -59.74°C. After the addition of modified MMT, the T_g value is not affected. All PCL bionanocomposites exhibited T_g of -61±2°C. Similar results were reported by various researchers for T_g of PCL nanocomposites [13, 24-27].

TGA analysis of PCL and its corresponding binary nanocomposites was carried out under nitrogen with a 10 °C/min heating rate (**Fig.3 (b)**). The characteristic temperature of degradation T_d10% (temperature at which 10% degradation occurred), are summarized in **Table 1**. Due to the addition of the MMT-ODA nanofiller, a raise of 82°C was recorded for the degradation temperature between neat PCL and PCL/MMT-ODA 5wt%. On the other hand, the thermal stability of the PCL/MMT-ODA nanocomposites was improved compared to pure PCL, and was expressed by an increase of the degradation. It is known that the clay layers may act as a heat barrier and consequently contribute to the overall thermal stability of the system. [15]

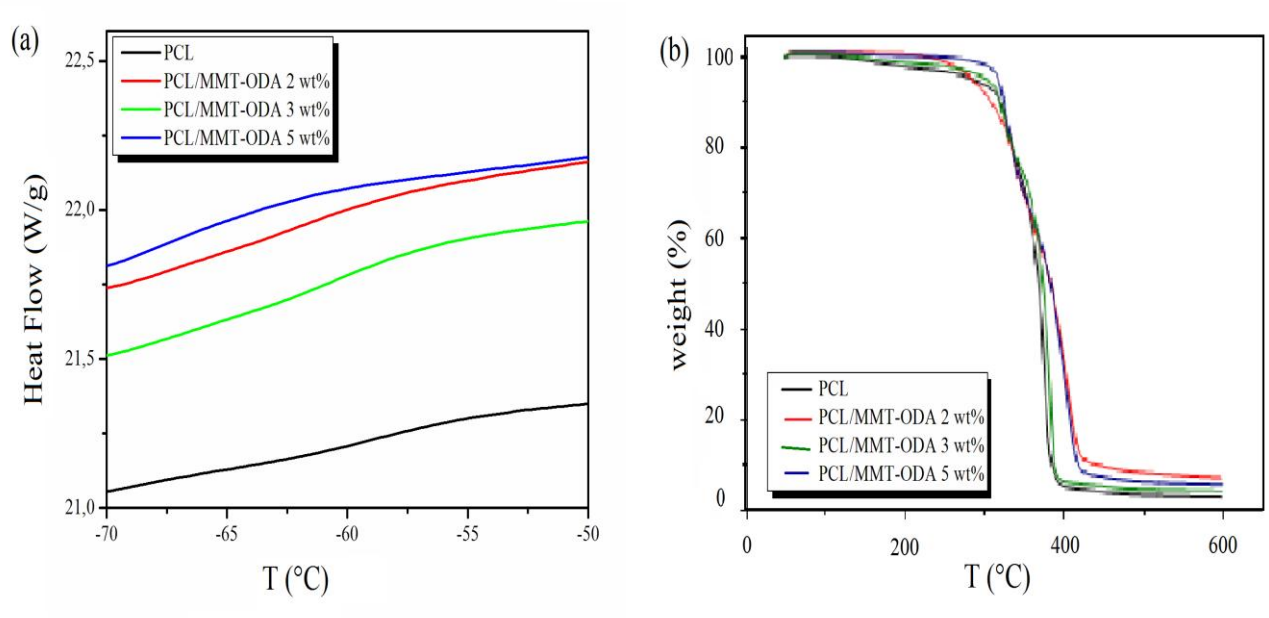

Fig. 3 DSC (a) and TGA (b) Thermograms of neat PCL and its nanocomposites.

Table 1 Thermal properties of PCL and its nanocomposites

	DSC	**TGA**
Samples	**Tg (°C)**	**T_d 10% (°C)**
PCL	-59.7	236
PCL/MMT-ODA 2 wt%	-61.4	305
PCL/MMT-ODA 3 wt%	-61.2	322
PCL/MMT-ODA 5 wt%	-63.2	318

3.3 Dielectric results

Fig. 4(a-d) and **Fig. 5(a-d)** show the dielectric permittivity (ε′) and the loss factor (ε″) for neat PCL and its bionanocomposites in the temperature range from -100 to 25°C, respectively.

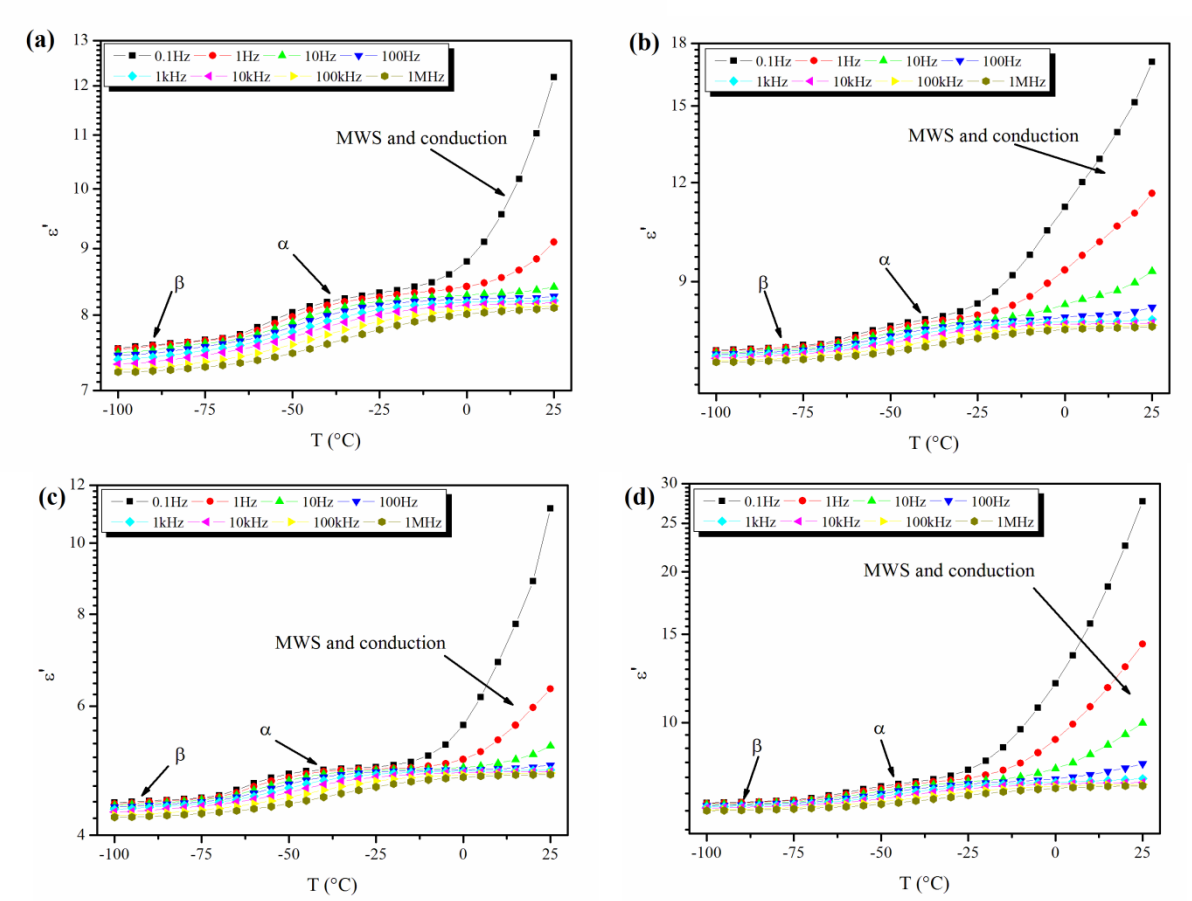

Fig. 4 The temperature dependence of the real part of dielectric permittivity ε′ for neat PCL (a), PCL/MMT-ODA 2 wt% (b), 3 wt% (c) and 5 wt% (d) at different frequencies.

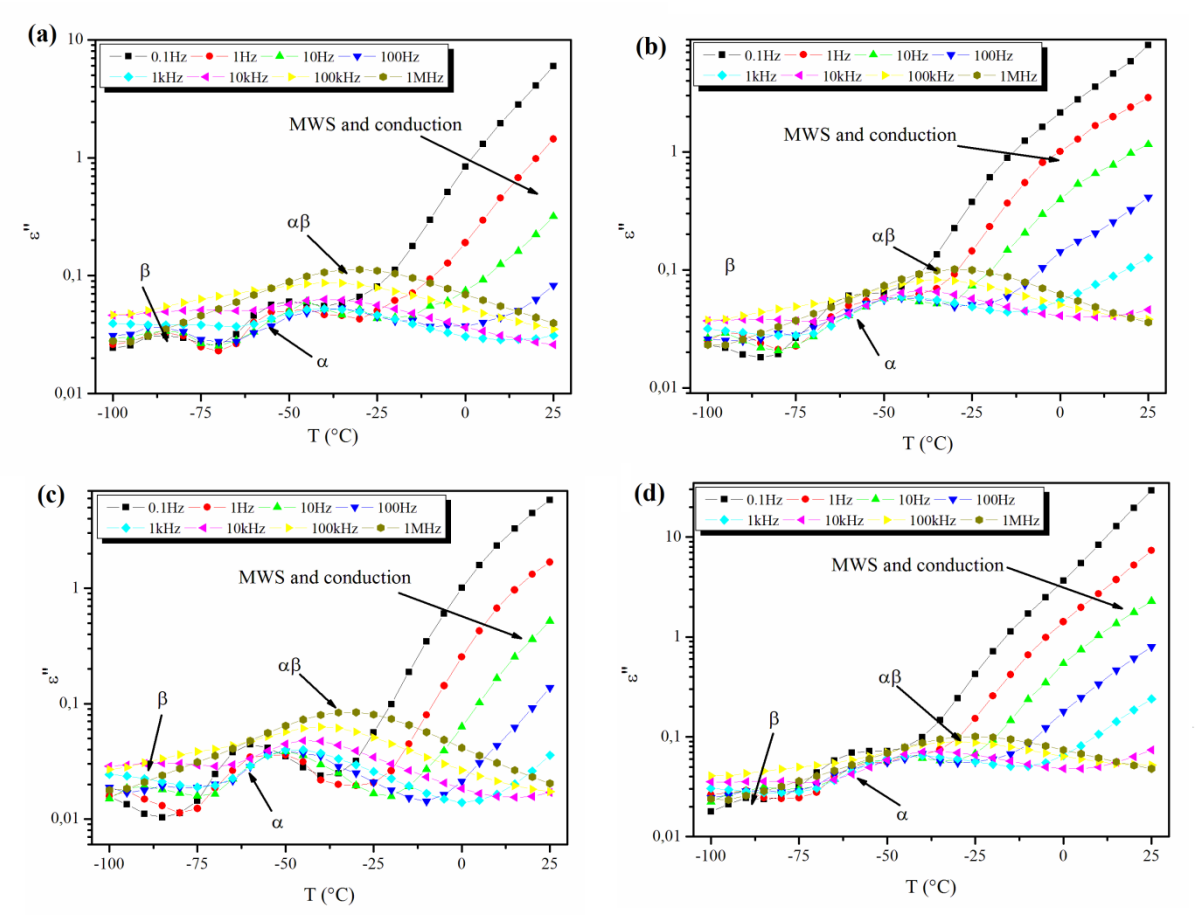

Fig. 5 The temperature dependence of the imaginary part of dielectric permittivity ε″ for neat PCL (a), PCL/MMT-ODA 2 wt% (b), 3 wt% (c) and 5 wt% (d) at different frequencies.

From the above isochronal curves, two temperature ranges are well distinguished, where dielectric relaxation processes are detected. At the lowest temperatures (−100 to -10 °C) the dielectric analysis results of all samples revealed the same dielectric phenomena [10-13, 20, 28]:

- The first process, observed at temperature between -100°C and -60°C, is associated with a β relaxation. This secondary mode is due to a localized mobility of fragments of PCL chains.

- The second peak appeared at the same frequency range as β mode and around the glass transition temperature T_g (≈-60°C) of PCL. This process indicates an α relaxation. This relaxation mode results from large-range motions "dipole-elastic process" corresponding to the microbrownian segmental movement of the chain.

- The third one is observed at higher frequencies (from 10 kHz to 1MHz) and for temperature between –50°C and -10°C, as shown in **Fig.5**. This new peak can be explained by the merging of α mode with the local β or the overlapping effect of these two relaxations. In addition, this resulting process was labeled αβ mode. The presence of this process was confirmed by the analysis reported by Grimau et al [10] and Bello et al [11]. These authors asserted that the merging of α and β modes into αβ process was evidenced at high temperature - high frequency range. Consequently, this strong overlap of the primary and secondary modes makes the calculated mean relaxation time of each mode from the maxima of the peak very difficult.

At higher temperatures (from -20 °C to 25 °C) and at low frequencies (from 0.1 Hz to 10 Hz), ε′ and ε″ exhibited a significant increase with temperature. This phenomenon can be explained by the increase of

mobility of charge carriers with temperature. According to previous works [10-12, 29], this important increase of permittivity noted at low frequency and higher temperature, is related to the ionic conduction phenomenon. Furthermore, in complex systems such as semicrystalline polymers with a conductive component, interfacial polarization is obscured by the increase of conductivity. This interfacial polarization is known as the Maxwell-Wagner-Sillars (MWS) and it is due to the accumulation of charges at the interfaces. In our case, MWS is due to the accumulation of charges at the interface between the amorphous and the crystalline regions of the semi-crystalline matrix and the matrix / reinforcement interface of nanocomposites.

The variation of real and imaginary parts of dielectric permittivity versus clay amounts, at room temperature and f = 10 Hz, are shown in **Fig.6**. The incorporation of clay in the PCL enhances the value of both dielectric constant (ε′) and the loss factor (ε″), except for the PCL/MMT-ODA 3 wt% nanocomposite which shows a decrease in the ε′ values. This decrease can be correlated to the homogeneous nanoparticles dispersion and the best interfacial adhesion between MMT-ODA and PCL matrix, in agreement with FTIR and XRD analyses.

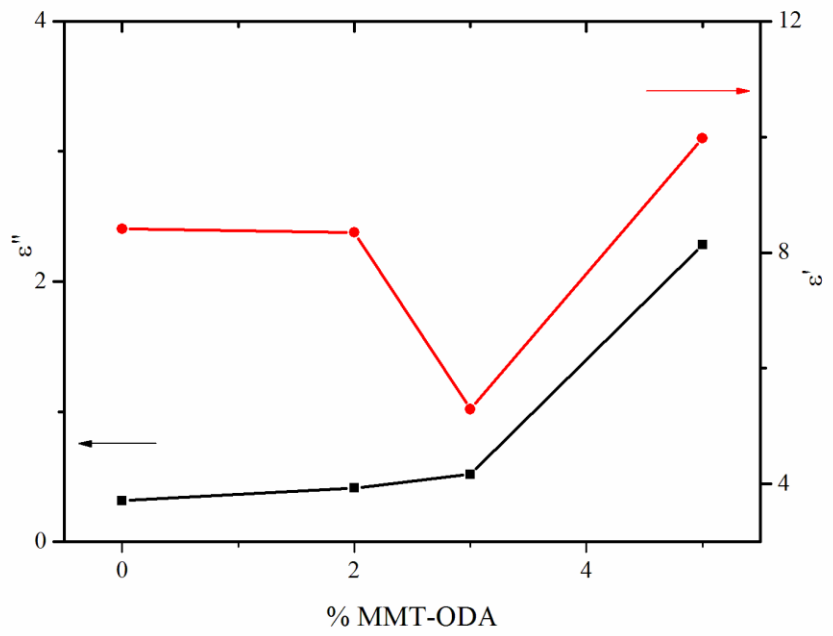

Fig. 6 Variation of real and imaginary parts of dielectric permittivity with clay amounts, at room temperature and f =10 Hz.

The relaxation patterns observed in dielectric spectra measured on neat PCL and its nanocomposites are complicated, due to the semicrystalline nature of PCL, the higher number of relaxation modes and its overlap. Therefore, it is necessary to model these relaxation data using the Havriliak and Negami empirical equation with the contribution of the conductivity term. We fit the real part ε′ of dielectric permittivity using the following HN equation:

$$\varepsilon'(\omega) = \frac{\sigma}{\varepsilon_0 \omega^N} + \sum_{k=1}^{n} \varepsilon_{k\infty} + \frac{\Delta\varepsilon_k \cos\theta_k}{[1+2(\omega\tau_k)^a \cos(\frac{a_k\pi}{2}) + (\omega\tau_k)^{2a_k}]^{\frac{b_k}{2}}} \quad (2)$$

$$\text{With } \theta_k = b_k \operatorname{atan}\left[\frac{(\omega\tau_k)^{a_k}\sin(\frac{a_k\pi}{2})}{1+(\omega\tau_k)^{a_k}\cos(\frac{a_k\pi}{2})}\right] \quad (3)$$

In this equation, the first term accounts for the conductivity contribution σ due to the space charges, where ε_0 note the permittivity of free space and N is the conductivity power. The second term is the superposition of the well-known Havriliak-Negami for n independent processes. Δε is the relaxation strength, ε_∞ is the permittivity at high frequency, τ is the relaxation time of the system, a is the shape parameter representing symmetrical distribution of relaxation time and b is the shape parameter of an asymmetric relaxation curve. The values of both a and b are between 0 and 1. These two coefficients act for the deviation from the Debye equation.

For each temperature, dielectric data can be split into two independent relaxation processes by fitting to the equation (2). At lower temperature, we confirm the presence of the β and α modes, while at higher temperature, we noticed the presence of the MWS polarization and the ionic conduction. **Fig.7 (a-d)** and **Fig.8 (a-d)** provide examples of the fitting process at T= -60°C and T=20°C, respectively.

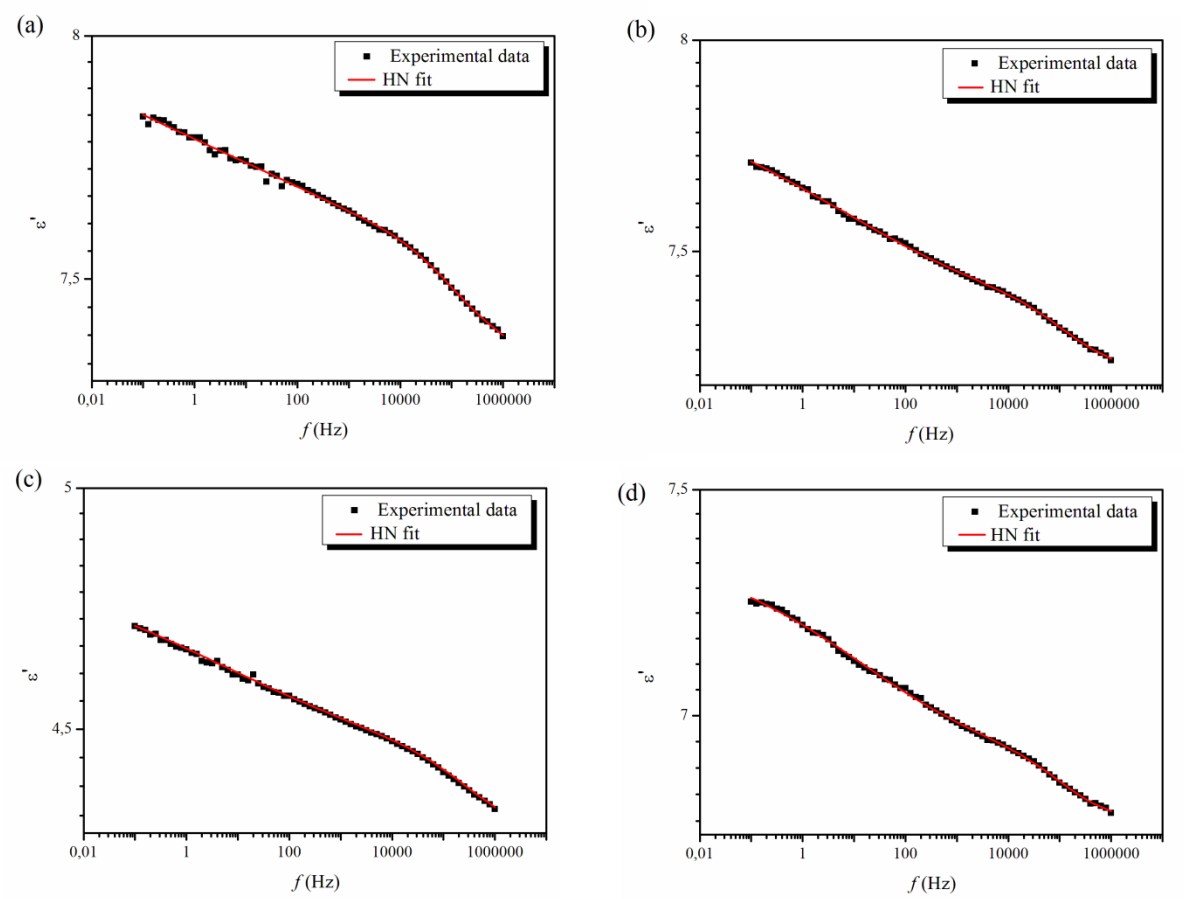

Fig. 7 Example of HN model fit of neat PCL (a) and its nanocomposites PCL/MMT-ODA 2 wt% (b), 3 wt% (c) and 5 wt% (d) at -60°C.

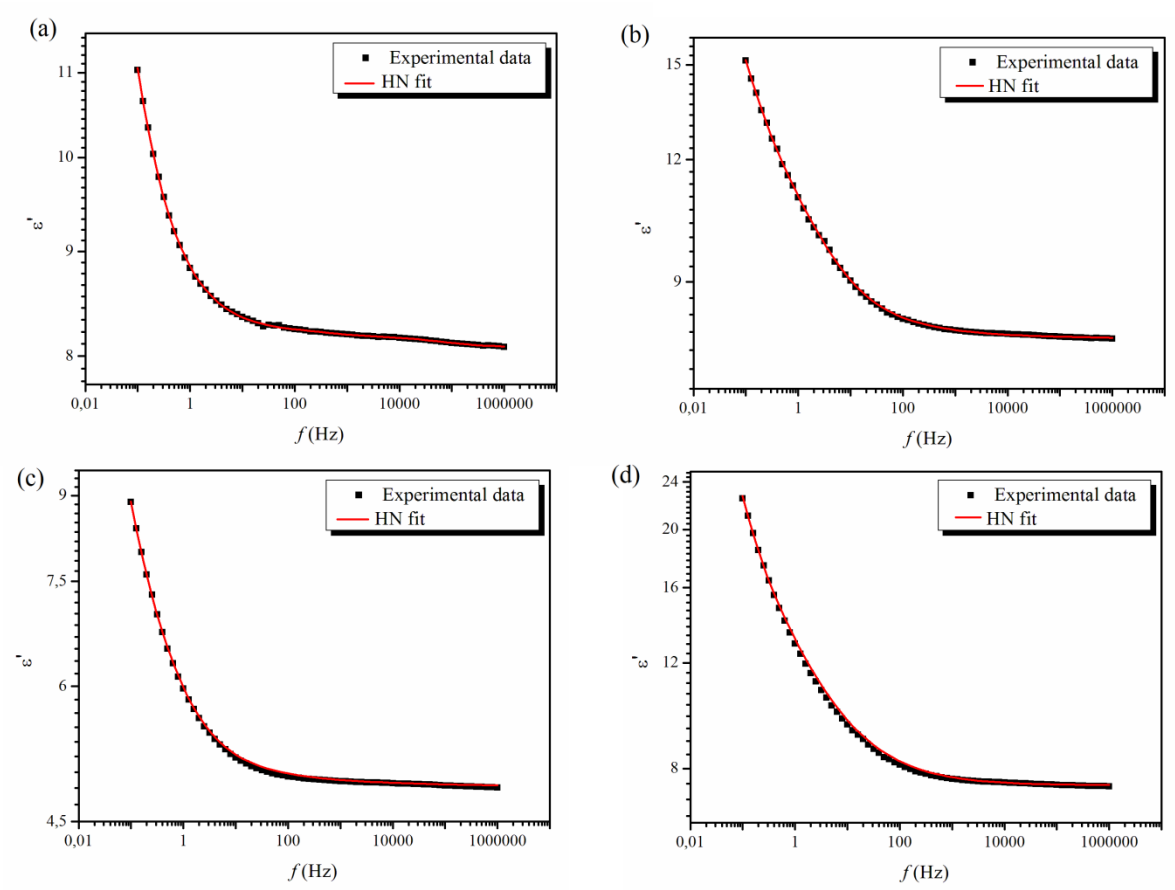

Fig. 8 Example of HN model fit of neat PCL (a) and its nanocomposites PCL/MMT-ODA 2wt% (b), 3wt% (c) and 5 wt% (d) at 20°C.

From the parameter τ evaluated by the fitting data, the relaxation times of each process τ_{max}, at which the dielectric loss is a maximum,can be calculated according to the following equation:

$$\tau_{max} = \tau \left[\frac{\sin\left(\frac{ab\pi}{2+2b}\right)}{\sin\left(\frac{a\pi}{2+2b}\right)} \right]^{\frac{1}{a}} \quad (4)$$

The relaxation time is related to viscous properties of the investigated dielectric. When plotting the ln (τ_{max}) versus the reciprocal temperature, all relaxations obeyed the Arrhenius linear behavior.

$$\tau(T) = A\exp\left[\frac{E_a}{k_B T}\right] \quad (5)$$

Where A is pre-exponential factor, E_a is the activation energy and k_B is the Boltzmann constant.

The obtained results for the activation energies of all processes are summarized in **Table 2**.

These values are in agreement with those reported in earlier works [10-13]. The activation energies of α and β relaxation modes for neat PCL are 0.18± 0.01 eV and 0.40 ± 0.01 eV, respectively. The nanocomposite samples exhibited the highest activation energies compared to neat PCL. This can confirm the reinforcing effect of

organo-modified clay. Also we note that the three nanocomposites have the same values of activation energies. Consequently, the local dynamics of PCL is unaffected by the increase of MMT-ODA nanoclay amount. It is confirmed by the DSC results that showed no changes in the glass transition temperature with the increase of clay content (**Table 1**). The neat PCL and its nanocomposites exhibit a T_g = -61±2 °C. This result is in good agreement with the studies of Kevin et al who reported that the segmental and the local dynamics are unaffected by the addition of clay [13]. Moreover, since the activation energy does not change, the size of the molecular unit responsible for the movement is the same and is not affected by the added clay.

On the other hand, the MWS polarization of pure matrix has activation energy 0.88 eV. Then, the E_a decrease when the clay amount varies from 0 to 3 wt%. This can be explained by the creation of new matrix/clay interfaces which make the accumulation of free charges carries easier. However, an increase of activation energy was detected at 5 wt% of added MMT-ODA. This increase can be due to agglomeration and poor dispersion of clay in polymer matrix at higher amount. This result goes hand in hand with the FTIR and XRD results shown for PCL/MMT-ODA 5wt% nanocomposite.

Table 2 Activation energies E_a (eV) for PCL matrix and PCL/MMT-ODA nanocomposites

Phenomenon	**Samples**	**E_a(eV)**
β relaxation	PCL	0.40 ± 0.01
	PCL/MMT-ODA 2 wt%	0.46 ± 0.01
	PCL/MMT-ODA 3 wt%	0.44 ± 0.01
	PCL/MMT-ODA 5 wt%	0.45 ± 0.01
α relaxation	PCL	0.18 ± 0.01
	PCL/MMT-ODA 2 wt%	0.24 ± 0.02
	PCL/MMT-ODA 3 wt%	0.26 ± 0.01
	PCL/MMT-ODA 5 wt%	0.26 ± 0.01
MWS	PCL	0.88 ± 0.01
	PCL/MMT-ODA 2 wt%	0.85 ± 0.02
	PCL/MMT-ODA 3 wt%	0.75 ± 0.03
	PCL/MMT-ODA 5 wt%	0.94 ± 0.03

Moreover, the dielectric strength Δε, obtained from the HN fit, is shown in **Fig.9**. This parameter is related to the number density of dipoles involved in the observed relaxation, as well as the magnitude of their dipole moment and how they are correlated [30, 31]. It is defined by:

$$\Delta\varepsilon = \varepsilon_s - \varepsilon_\infty = \frac{N\mu^2}{3k_BT} \quad (6)$$ where ε_s and ε_∞ are, respectively, the dielectric permittivity in the low and high frequency limit, N is the concentration of dipoles and the dipole moment, μ is the mean squared dipole moment and k_B is Boltzmann's constant.

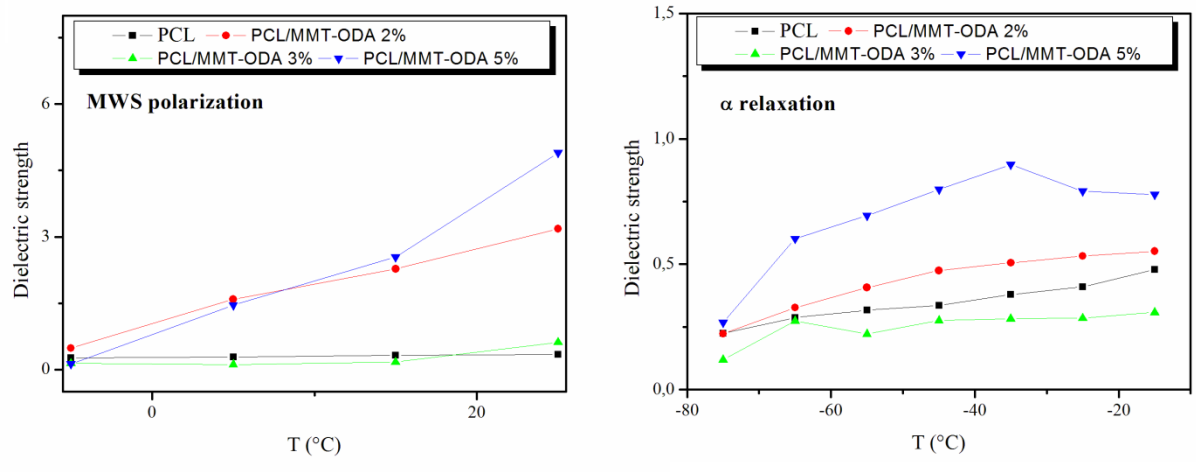

Fig. 9 Dielectric relaxation strength for the interfacial polarization MWS and α relaxation.

For α relaxation, the relaxation strength Δε, for all samples, slightly increases at higher temperature. Then, the supplementation of 1wt% of organo-modified clay increases the dipole moment of the polymeric matrix and their mobility with the applied electric field. In fact, the organomodified clay (having polar groups) plays an important role in increasing the dipoles moment μ and polarization strength Δε [13]. For PCL/MMT-ODA 3 wt%, we noticed a decrease in the relaxation strength values. This result can come from the increase in the degree of crosslinking, thus reducing the polarization capacity of the dipoles [32]. For 5 wt% clay amount, the relaxation strength is increased. The presence of agglomerates increases the dipoles mobility of the chains by making the PCL matrix freer.

For the interfacial polarization MWS, the following observations could be pointed out:

- Generally, the relaxation strength increases with the temperature. It is due to the accumulation of free charges at the interfaces, thus increasing the ability of the dipoles to be polarized. This phenomenon is amplified by temperature rise which accelerate the charge carrier mobility [33, 34].

- The presence of clay increase the relaxation strength Δε then decrease with 3 wt% of MMT-ODA. The decrease of Δε explains the strong adhesion of the interfacial region (matrix/reinforcement) and therefore reducing the ability of the dipoles to relax [32, 33]. So, the PCL/MMT-ODA 3 wt% presents the best and strongest adhesion between PCL matrix and organo-modified clay. For PCL/MMT-ODA 5 wt%, the relaxation strength is increased. It can be due to the increase of number of charges carries and their mobility. With a higher clay content, the agglomerates prevent the penetration of the polymer into the organo-clay gallery, making the adhesion between PCL and MMT-ODA very weak.

3.4 Temperature dependent conductivity studies

The study of ac conductivity elucidates the time-dependent charge movements, which can lead to conductivity and dielectric relaxation phenomena. This analysis may offer further insight into the distribution of the electric fields in the system and the field-induced perturbations. The frequency dependence of the ac conductivity (σ′) for PCL and its nanocomposites, in the temperature range from -100 °C to 25 °C, is plotted in **Fig.10**.

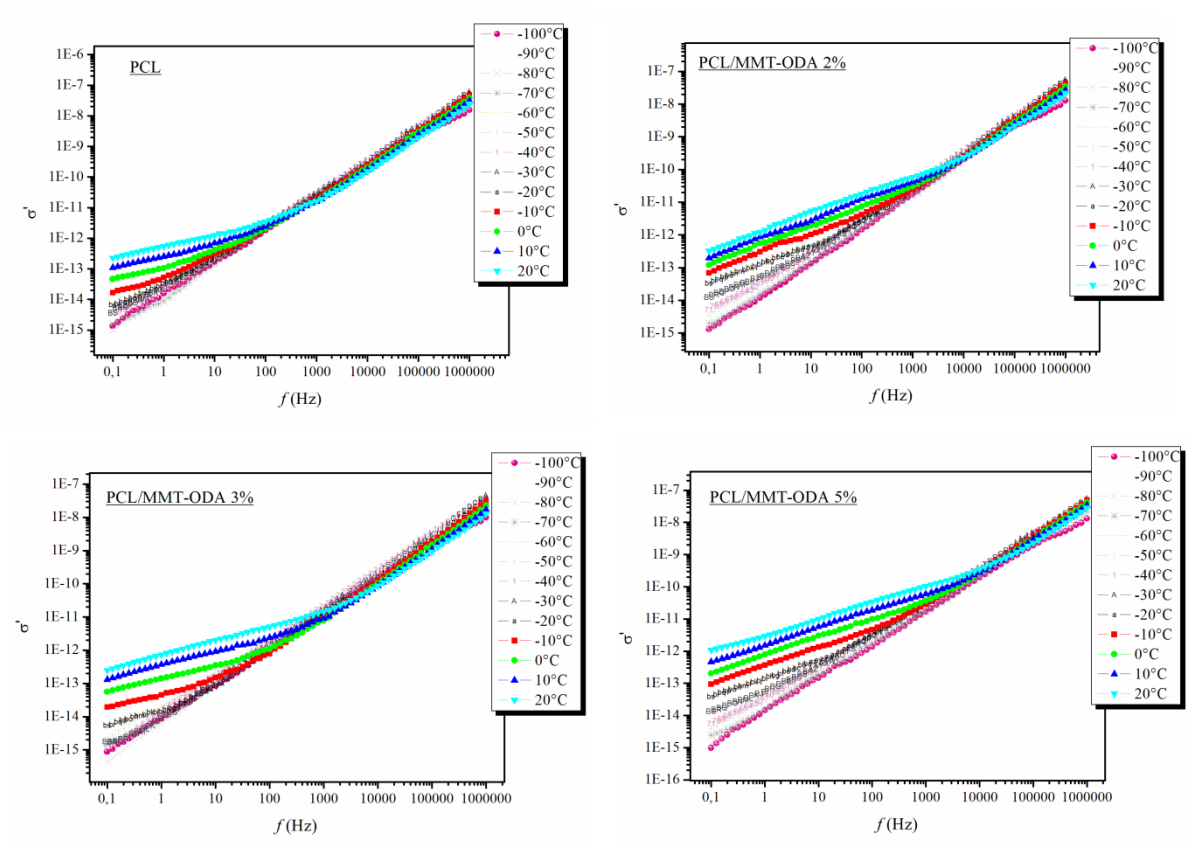

Fig. 10 The ac conductivity (σ_{ac}) versus frequency for pure PCL and its nanocomposites.

Generally, the curve of electrical conductivity can be devised in two distinct regions i.e. the low frequency plateau region and high frequency dispersion region. The first region, shown at low frequency, is associated with the dc conductivity (σ_{dc}) in which the conductivity underlines a frequency independent plateau with an almost constant value. However, the conductivity is found to increase with increasing frequency in the second region, following a power law ($A\omega^s$). At low frequencies, the random distribution of the ionic charge carriers via the activated jump gives rise to a frequency independent conductivity. While at higher frequencies, the conductivity dispersion roughly increases according to the power law at even higher frequencies. Therefore, the Jonscher's law can describe the expression of conductivity:

$$\sigma_{ac}(\omega, T) = \sigma_{dc}(T) + A(T)\omega^{s(\omega,T)} \quad (7)$$

where σ_{dc} is the direct current conductivity, ω is the angular frequency, the A and s parameters are constants dependent on temperature. The A parameter reflects the polarizability and s the interaction degree between mobile ions and the surrounding environment [32, 35].

In **Fig.10**, it is clear that there is no σ_{dc} plateau in the conductivity curves in the frequency and temperature ranges used in our study. At low frequency, the values of σ′ increase slightly with both frequency and temperature. Then, at higher frequencies, the charge carrier's displacement is reduced, all the isotherms collapse and the frequency dependence of conductivity is nearly the same. This behavior is known as the nearly constant loss (NCL) regime. It is related to the frequency range where the ε* value is nearly independent of frequency [36].

In order to determine the ac conduction mechanism for the present nanocomposites, we analyzed the variation of the exponent s as a function of temperature (**Fig.11**). The values of s are extracted from the slopes of the plot Ln σ_{ac} versus angular frequency (ω). As it can be seen, this parameter depends of temperature and

clay content. We note that PCL/MMT-ODA 3wt% has the highest values of s, while PCL/MMT-ODA 5wt% has the smallest values. As the exponent s presents the degree of interaction between the mobile ions and the surrounding environment, we conclude that the nanocomposite with 3 wt% of clay has the lowest conductivity and thus 5wt% has the highest conductivity values. This is in good accordant with the results observed on the dielectric part.

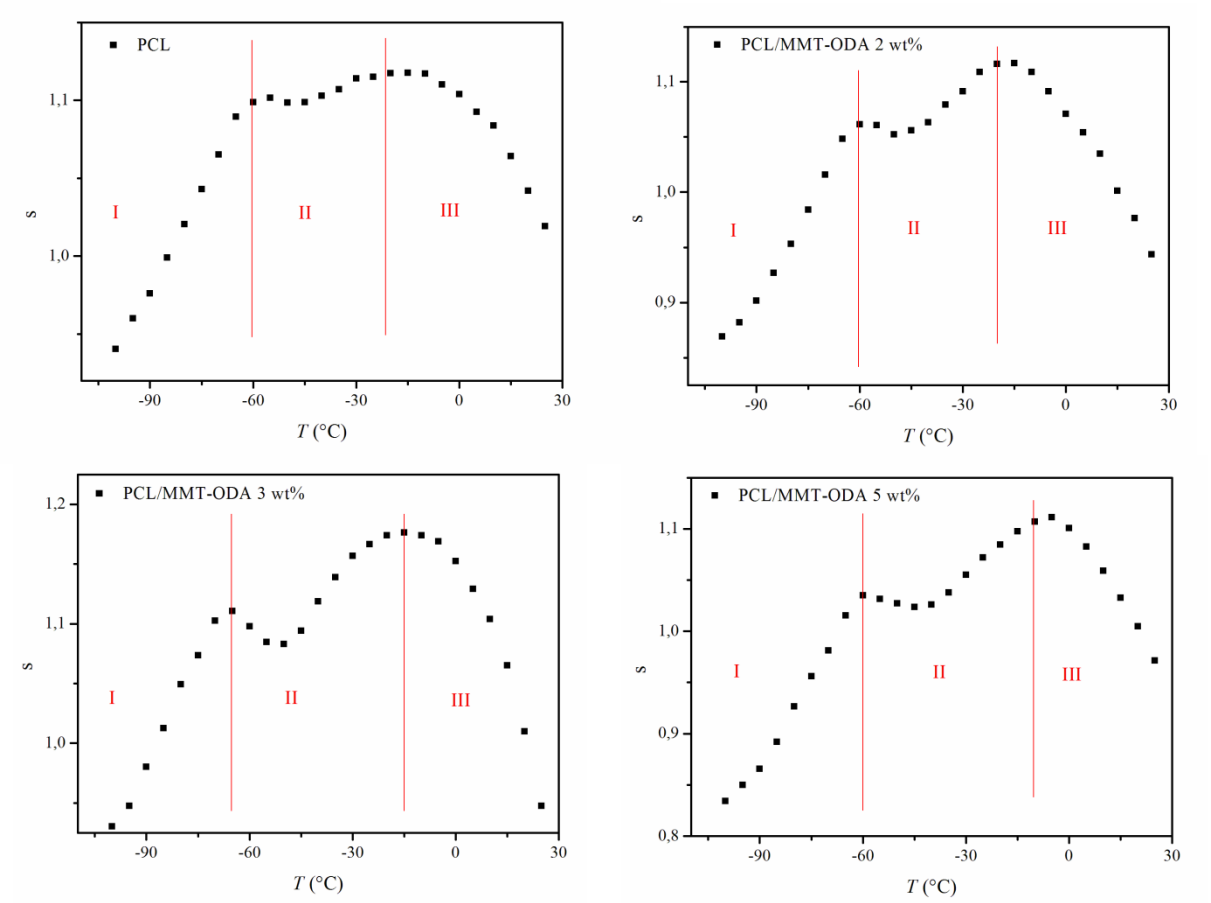

Fig. 11 Temperature dependency of the exponent s for PCL matrix and its nanocomposites.

Moreover, the value of s is significantly affected by temperature, showing the same dependence for all the nanocomposites. Below the glass transition temperature, s increases slightly with temperature. Then we note that the mechanism conduction changes at the glass temperatures, where s decreases to a minimum value then increases. And after -20°C, it decreases again. Thus, several theoretical models can be invoked to interpret the AC conduction mechanism for the PCL and its nanocomposites (**Fig.11**):

(1) The small polaron tunneling (SPT) model: the exponent s increases with temperature increase [37, 38]. This model can be established in a covalent solid if the addition of a charge carrier to a site causes a high degree of distortion of the local lattice. This model is applicable to the obtained results in the phase I (-100°C≤T≤-60°C) where the local β mode relaxation is depicted.

(2) The overlapping polaron tunneling (OLPT) model: the s values decreases to a minimum value then increases, with the temperature increase [37, 39]. Wherever the polaron energy is derived from polarization changes in the deformed lattice as in ionic crystals, A mechanism for polaron tunneling has been suggested by Long [40]. The consequent excitation is called a large or dielectric polaron. Due to the long range of the Coulomb interaction, its well extends over many interatomic distances and overlap with those of other sites. This model is in harmony with the obtained results in the phase II (-60°C≤T≤-20°C) where the segmental α relaxation is depicted.

(3) The correlated barrier hopping (CBH) model: when the temperature increases, the values of s decreases [37, 41]. The CBH model can be applied for many organic–inorganic materials. In this model, the conduction can be created via a single polaron (or bipolaron) hopping process beyond the Coulomb barrier separating two defect centers. The obtained results in phase III (-20°C≤T≤25°C) is in good agreement with this model, where the MWS polarization is defined.

It is clear that the values of exponent s exceed the universal one (s = 0.8-1). Similar results have been found in some nanocomposite systems, comprising conducting and insulating phase network. Ortiz-Serna et al [36] explained this discordance by weak contacts between the fillers.

Moreover, according to the jump relaxation model [42, 43], the exponent s can be related with the back hop rate (B_r) and the site relaxation rate (S_r) by the following expression:

$$s = \frac{B_r}{S_r} \tag{8}$$

The back hop defines the backward motion of a hopping ion to its initial site. It can be induced by the Coulomb repulsive interaction among mobile ions. The site relaxation (S_r) is known as the shift of a site potential minimum to the position of the hopping ion due to the rearrangement of neighboring ions [42, 44].

If the backward hopping is slower than the site relaxation, the exponent s has a value lower than one. However, if the backward hopping is faster than the site relaxation, the s value is higher than one.

Consequently, we conclude that the values of s greater than one are due to the presence of the Columbic repulsion between the mobile ions or a bad site for the next hop. [42]

4. Conclusions

We focused on the dielectric and electrical properties of bio-nanocomposites based on poly (ε-caprolactone) (PCL) as a matrix reinforced by organomodified clay (MMT-ODA) prepared by in-situ ROP. These properties were investigated via broadband dielectric relaxation spectroscopy in the frequency range from 1 Hz to 1 MHz and in the temperature range from -100°C to 25°C. The relaxation patterns observed in dielectric spectra measured were complicated, due to the semicrystalline nature of PCL, the higher number of modes and its strong overlap. So, it was necessary to model these relaxation data using the Havriliak and Negami empirical equation plus a conductivity term. From the resulting parameters of HN fit and the evolution of the activation energies, the effect of clay on PCL dielectric properties was investigated. The MWS polarization was strongly affected by the addition of MMT-ODA clay and we noticed an agglomeration and poor dispersion of clays in the polymer matrix at a higher amount of added clay (5 wt%). This result was in good agreement with the FTIR and XRD results that showed good dispersion of the clay nano-particles in the neat PCL matrix until 3 wt% of organo-modified clay, while, for 5 wt%, a poor dispersion and an agglomeration phenomenon were detected. However, the local dynamics of PCL was unaffected by the increase of the nano-clay content, followed by the same DSC values of T_g temperature for all samples. On the other hand, the frequency-dependent ac conductivity of PC and its nanocomposites was analyzed in term of Jonscher's law. And the temperature variation of the exponent s proposed many theoretical models to interpret the ac conductivity mechanism: SPT model (-100°C≤T≤-60°C), OLPT model (-60°C≤T≤-20°C) and CBH model (-20°C≤T≤25°C). For their ability to store/dissipate energy under exposure to an electric field, these eco-friendly bio-nanocomposites reinforcing with clay are appropriate for many applications, such as fuel cell lithium ion batteries and photovoltaic that the fluoropolymers are used.

Acknowledgments

The authors appreciate the financial support of Moroccan and Tunisian committee in the framework of the program of collaboration of scientific exchange; contact grant number: 17TM20

Funding

This work has no source of funding.

Availability of Data and Materials

The datasets generated during and/or analyzed during the current study are available from the corresponding author on request.

Competing Interests

The authors declare that they have no competing intetests.

References

[1] Usman MS, Ibrahim NA, Shameli K, Zainuddin N, Wan Yunnus WMZ; Copper nanoparticles mediated by chitosan: Synthesis and characterizationvia chemical methods, Molecules 2012, 17:14928.

[2] Ahmad MB, Gharayebi Y, Salit MS, Hussein MZ, Shameli K; Comparison of in situ polymerization and solution-dispersion techniques in the preparation of polyimide/montmorillonite (MMT) nanocomposites, Int. J. Mol. Sci. 2011, 12:6040.

[3] Ahmad MB, Lim JJ, Shameli K, Ibrahim NA, Tay MY; Synthesis of silver nanocomposites in chitosan, gelatin and chitosan/gelatin bionanocomposites by a chemical reducing agent and their characterization, Molecules 2011, 16:7237.

[4] Shameli K, Ahmad MB, Shabanzadeh P, Al-Mulla EAJ, Zamanian A, Abdollahi Y, Jazayeri SD, Elli M, Jalilian FA, Haroun RZ; Effect of curcuma longa tuber powder on size of silver nanoparticles prepared by green method, Res. Chem. Intermed. 2013, 40:1313.

[5] Bordes P, Pollet E, Avérous L; Nano-composites: biodagradable polyester/nanoclay systems, Prog. Polym. Sci. 2009, 34:125.

[6] Dong Y, Bhattacharyya D; Effects of clay type, clay/compatibiliser content and matrix viscosity on the mechanical properties of polypropylene/organoclay nanocomposites, Compos Part A Appl. Sci. Manuf. 2008, 39:1177.

[7] Calcagno CIW, Mariani CM, Teixeira SR, Mauler RS; The role of the MMT on the morphology and mechanical properties of the PP/PET blends, Compos. Sci. Technol. 2008, 68:2193.

[8] Santos KS, Liberman SA, Oviedo MAS, Mauler RS; Optimization of the mechanical properties of polupropylene-based nanocomposite via the addition of a combination of organoclays, Compos. Part A Appl. Sci. Manuf. 2009, 40:1199.

[9] Nishida H, Tokiwa Y; Distribution of poly(β-hydroxy-butyrate) and poly(ε-caprolactone) aerobic degrading microorganisms in different environments, J. Environ. Polym. Degrad. 1993, 1:227.

[10] Grimau M, Laredo E, Pérez MC, Bello A; Study of dielectric relaxation modes in poly(ε-caprolactone): Molecular weight, water sorption and merging effects, J. Chem. Phys. 2001, 114:6417.

[11] Bello A, Laredo E, Grimau M; Comparison of analysis of dielectric apectra of PCL in the ε^* and the M^* formalism, J. Non-Cryst. Solids 2007, 353:4283.

[12] Woo HJ, Majid SR, Arof AK; Conduction and thermal properties of a proton conducting polymer electrolyte based on poly(ε-caprolactone), Solid. State Ionics 2011, 199-200:14.

[13] Kevin AM, Hongyi Y, Alamgir K, Chad RS; Polymer chain dynamics in intercalated poly(ε-caprolactone)/nanoplatelet blends, Macromolecules 2013, 46:2235.

[14] Avella M, Bondioli F, Cannillo V, Pace ED, Errico ME, Ferrari AM, Focher B, Malinconico M; Poly (ε-caprolactone)-based nanocomposites: influence of compatibilization on properties of Poly(ε-caprolactone)-silica nanocomposites, Comp. Sci. and Tech. 2006, 66:886.

[15] Sengwa RJ, Choudhary S, Sankhla S; Dielectric properties of montmorillonite clay filled poly(vinyl alcohol)/poly(ethylene oxide) blend nanocomposites, Compos. Sci. Technol. 2010, 70:1621.

[16] Elghaoui H, Raihane M, Rhouta B, Bitinis N, Carlmark A, Arroyo M, Verdejo R, Lopez-Manchado MA, Lahcini M; Bismuth complex catalysts for the in situ preparation of polycaprolactone/silicate bionanocomposites, Polym. Inter. 2014, 63:709.

[17] Nirmala R, Nam KT, Park DK, Woo-il B, Navamathavan R, Kim HY; Structural, thermal, mechanical and bioactivity evaluation of silver-loaded bovine bone hydroxyapatite grafted poly([epsilon]-caprolactone) nanofibers via electrospinning, Surface and Coating Technology 2010, 205:174.

[18] Woo HJ, Arof AK; Vibrational studies of flexible solid polymer electrolyte based on PCL-EC incorporated with proton conducting NH_4SCN, Spectroch. Act. Part A: Molec. and Biomolec. Spectros. 2016, 161:44.

[19] Elzein T, Nasser-Eddine M, Delaite C, Bistac S, Dumas P; FTIR study of polycaprolactone chain organization at interfaces, J. Collo. and Inter. Sci. 2004, 273:381.

[20] Ghasemi-Mobarakeh L, Prabhakaran MP, Morshed M, Nasr-Esfahani MH, Ramakrishna S; Bio-functionalized PCL nanofibrous scaffolds for nerve tissue engineering, Mater. Sci. and Eng. C 2010, 30:1129.

[21] Then YY, Ibrahim NA, Yunnus WMZ; Enhancement of tensile strength and flexibility of polycaprolactone/tapioca starch blends by octadecylamine modified clay, J. Polym. Environ. 2011, 19:535.

[22] Emad A, Al-Mulla J; A new biopolymer-based polycaprolactone/starch modified clay nanocomposite, Cellulose Chem. Technol. 2014, 48:515.

[23] Salehiyan R, Yussuf AA, Hanani NF, Hassan A, Akbari A; Polylactic acid/polycaprolactone nanocomposite: influence of montmorillonite and impact modifier on mechanical, thermal and morphological properties, J. of Elast. and Plast. 2015, 47:69.

[24] Yahiaoui F, Benhacine F, Ferfera-Harrar H, Habi A, Hadj-Hamou AS, Grohens Y; Development of antimicrobial PCL/nanoclay nanocomposite films with enhanced mechanical and water vapor barrier properties for packaging applications, Polym. Bull. 2014, 72:235.

[25] Lepoittevin B, Devalckenaere M, Pantoustier N, Alexandre M, Kubies D, Calberg C, Jerome R, Dubois P; Poly (ε-caprolactone)/clay nanocomposites prepared by melt intercalation : mechanical, thermal and rheological properties, Polym. 2002, 43:4017.

[26] Labidi S, Azema N, Perrin D, Cuesta JML; Organo-modified montmorillonite/ poly(ε-caprolactone) nanocomposites prepared by melt intercalation in a twin-screw extruder, Polym. Degrad. Stab. 2010, 95:382.

[27] Rittigstein P, Torkelson JM; Polymer-nanoparticle interfacial interactions in polymer nanocomposites: confinement effects on glass transition temperature and suppression of physical aging, J. Polym. Sci. Part B Polym. Phys. 2002, 44:2935.

[28] Hammami H, Arous M, lagache M, Kallel A; Study of the interfacial MWS relaxation by dielctric spectroscopy in unidirectional PZT fibers/epoxy resin composites, J. Allo. and Comp. 2007, 430:1.

[29] Wurm A, Soliman R, Schick C; Early stages of polymer crystallization- a dielectric study, 44 (2003) 7467.

[30] Tsangaris GM, Psarras GC; The dielectric response of a polymeric three-component composite, J. Mater. Sci. 1999, 34:2151.

[31] Kremer F, Schonhals A; Broadband Dielectric Spectroscopy, 1st ed.; Springer-Verlag: New York (2003).

[32] Ladhar A, Arous M, Boufi S, Kallel A; Molecular dynamics of poly (styrene-co-2-ethyl hexylacrylate) copolymer/ cellulose nanocrystals nanocomposites investigated by dielectric relaxation spectroscopy : Effect of the silane content, J. of Mol. Liq. 2016, 224:515.

[33] Arous M, Ben Amor I, Boufi S, Kallel A; Experimental study on dielectric relaxation in alfa fiber reinforced epoxy composites, J. of Appl. Polym. Sci. 2007, 106:3631.

[34] Ghallabi Z, Rekik H, Boufi S, Arous M, Kallel A; Effect of the interface treatement on the dielectric behavior of composite materials of unsaturated polyester reinforced by alfa fiber, J. Non-Cryst. Solid. 2010, 356:684.

[35] Chen RH, Chen LF, Chia CT; Impedance spectroscopic studies on congruent $LiNbO_3$ single crystal, J. Phys. Condens. Mat. 2007, 19:086225.

[36] Ortiz-Serna P, Carsí M, Redondo-Foj B, Sanchis MJ; Electrical conductivity of natural rubber–cellulose II nanocomposites, J. Non-Cryst. Solid. 2014, 405:180.

[37] Ben Bechir M, Karoui K, Tabellout M, Guidara K, Ben Rhaiem A; Alternative current conduction mechanisms of organic-inorganic compound [N(CH3)3H]2ZnCl4, J. of Appl. Phys. 2014, 115:153708.

[38] Gudmundsson JT, Svavarsson HG, Gudjonsson S, Gislason HP; Frequency-dependent conductivity in lithium-diffused and annealed GaAs, Phys. B 2003, 340:324.

[39] Megdiche M, Perrin-pellegrino C, Gargouri M; Conduction mechanism study by overlapping large-polaron tunnelling model in SrNiP2O7 ceramic compound, J. Alloys Compd. 2014, 584:209.

[40] Long AR; Frequency-dependent loss in amorphous semiconductors, Adv. Phys. 1982, 31:553.

[41] Mollah S, Som KK, Bose K, Chaudri BK; AC conductivity in Bi4Sr3Ca3CuyOx (y=0-5) and Bi4Sr3Ca3zLizCu4Ox (z=0.1-1.0) semiconducting oxide glasses, J. Appl. Phys. 1993, 74:931.

[42] Ravi M, Song S, Gu K, Tang J, Zhang Z; Electrical properties of biodegradable poly (ε-caprolactone): Lithium thiocyanate complexed polymer electrolyte films, Mater. Sci. and Eng. B 2015, 195:74.

[43] Funke K; Ion transport in fast ion condutors- spectra and models, Sol. Stat. Ion. 1997, 96:27.

[44] Le Meins JM, Bohnke O, Courbion G; Ionic conductivity of crystalline and amorphous $Na_3Al_2(PO_4)_2F_3$, Sol. Stat. Ion. 1998, 111:67.

Figure caption

Fig. 1 FTIR spectra recorded at room temperature of neat PCL and its nanocomposites

Fig. 2 XRD diffractograms for MMT-Na^+ and MMT-ODA (a) and PCL/ODA-MMT nanocomposites (b)

Fig. 3 DSC (a) and TGA (b) Thermograms of neat PCL and its nanocomposites

Fig. 4 The temperature dependence of the real part of dielectric permittivity ε′ for neat PCL (a), PCL/MMT-ODA 2 wt% (b), 3 wt% (c) and 5 wt% (d) at different frequencies

Fig. 5 The temperature dependence of the imaginary part of dielectric permittivity ε″ for neat PCL (a), PCL/MMT-ODA 2 wt% (b), 3 wt% (c) and 5 wt% (d) at different frequencies

Fig. 6 Variation of real and imaginary parts of dielectric permittivity with clay amounts, at room temperature and f =10 Hz

Fig. 7 Example of HN model fit of neat PCL (a) and its nanocomposites PCL/MMT-ODA 2 wt% (b), 3 wt% (c) and 5 wt% (d) at -60°C

Fig. 8 Example of HN model fit of neat PCL (a) and its nanocomposites PCL/MMT-ODA 2wt% (b), 3wt% (c) and 5 wt% (d) at 20°C

Fig. 9 Dielectric relaxation strength for the interfacial polarization MWS and α relaxation

Fig. 10 The ac conductivity (σ_{ac}) versus frequency for pure PCL and its nanocomposites

Fig. 11 Temperature dependency of the exponent s for PCL matrix and its nanocomposites